

Special Collection

Sustainably Scaled Electrochemical Synthesis of 3-Propyladipic Acid in Line with Fluctuating Grid Supply

Roland J.-R. Bednarz^{+, [a]}, Pilar Jiménez-Meneses^{+, [b]}, Annika S. Gold,^[a] Damián Monllor-Satoca,^[b] Andreas Stenglein,^[a] Roberto Gómez,^{*, [b]} and Siegfried R. Waldvogel^{*, [a, c]}

Chemical production is a significant contributor to global climate change, which expedites the growing demand for transitioning to more sustainable and climate-friendly methodologies. Ideally this should include high compatibility with the fluctuating electricity supply which results from renewable energy sources in the electrical grid. Here we show an electrochemical path for the 3-propyladipic acid synthesis from 4-propylcyclohexanol implementing a semi-technical electrochemical continuously stirred tank reactor. Following a *Design*

of Experiments approach, we found a strong influence of the biphasic electrolyte mixing and the continuous feeding in of the substrate. By switching to an electrolyte recirculation mode and efficient mixing, the isolated product yield could be increased up to 31% for a 10 L total reaction volume, indicating the potential for further scale-up into the technical range. This reaction proceeds while forming several by-products, which have not been fully described yet. A proposal for the formation mechanism is included.

Introduction

The continuing use of fossil fuels and the net emission of greenhouse gases are among the predominant industrial issues of this century. With a predicted annual world population growth of 0.9% on average until 2035^[1] and an exceeding primary energy demand, one-world chemistry has been advocated as an important approach with respect to the global ecological footprint.^[2] Organic electrosynthesis appears as a promising approach to make large-scale chemical reactions more environmentally benign while offering precise control

over reaction conditions.^[3] The prominent feature of this methodology is the use of electrons as green reagent, if renewable electricity is used.^[4] Additionally, the direct use of electrons significantly decreases reaction waste by replacing oxidizers and reductants with reusable electrodes. The electrochemical process becomes inherently safe as the reaction stops once the electrical current flow ends. A further advantage is the adjustable power consumption, via the employed number of cells or the current density, taking into account variances in the grid supply.^[5] Moreover, electrochemistry can offer superior or novel synthetic methods^[6] and galvanostatic processes enable easy scalability (vide infra).^[7]

Some electro-synthetic processes require low current densities to prevent product degradation, which leads to lower space-time-yields. One classic remedy is enlarging the active electrode surface area, which is realizable with foam electrodes or increased electrode size. Besides simply using two larger planar electrodes, electrode stacks with bipolar or monopolar connections are not necessarily limited in number, allowing for increases in electrode size with only minor increases in the cell volume.^[8]


Additionally, the use of biomass as a feedstock instead of fossil-fuels is another pathway to increase the sustainability of chemical processes.^[9] This change would allow for a decrease in greenhouse gas emissions by more than 60%,^[10] compared to traditional synthesis pathways of adipic acid. Previous work by Schutyser et al. illustrated this point, reporting the depolymerization and hydrogenation of lignin to 4-alkylcyclohexanols, such as 4-propylcyclohexanol.^[11] Consequently, 4-propylcyclohexanol may become abundantly available when lignin is heavily used as a regenerative feedstock in the future. Therefore, this study focuses on the anodic oxidation of this cyclic alcohol at activated nickel foam electrodes, with a focus on the derived scale-up. Nickel oxyhydroxide anodes regenerate during the electrolysis in alkaline media and have been employed for lignin degradation.^[12] The electrochemical oxidation of

[a] R. J.-R. Bednarz,⁺ A. S. Gold, A. Stenglein, Prof. Dr. S. R. Waldvogel
Department of Chemistry
Johannes Gutenberg University
Duesbergweg 10–14
55128 Mainz (Germany)
E-mail: waldvogel@uni-mainz.de
Homepage: <http://www.aksw.uni-mainz.de/>


[b] Dr. P. Jiménez-Meneses,⁺ Dr. D. Monllor-Satoca, Prof. Dr. R. Gómez
Institut Universitari d'Electroquímica i Departament de Química Física
Universitat d'Alacant
Apartat 99
E-03080 Alicante (Spain)
E-mail: roberto.gomez@ua.es
Homepage: <https://web.ua.es/gfes/>

[c] Prof. Dr. S. R. Waldvogel
Institute of Biological and Chemical Systems – Functional Molecular Systems (IBCS-FMS)
Hermann-von-Helmholtz-Platz 1
76344 Eggenstein-Leopoldshafen (Germany)

[⁺] These authors contributed equally to this work.

 Supporting information for this article is available on the WWW under <https://doi.org/10.1002/cctc.202300606>

 This publication is part of a Special Collection on "Holistic Development of Electrochemical Processes for Industrial Systems"

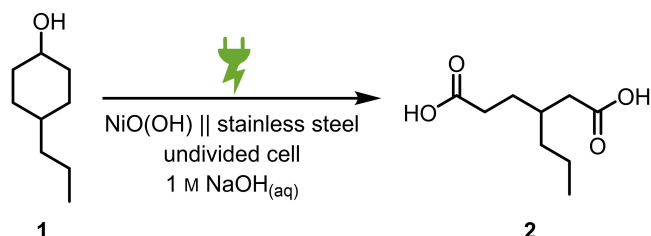
 © 2023 The Authors. ChemCatChem published by Wiley-VCH GmbH. This is an open access article under the terms of the Creative Commons Attribution License, which permits use, distribution and reproduction in any medium, provided the original work is properly cited.

alcohols has previously been investigated by Schäfer et al., who showed the successful oxidation of alcohols at such nickel oxyhydroxide anodes in caustic soda.^[13] Based on these results, Lyalin and Petrosyan electrochemically synthesized adipic acid from cyclohexanol with a yield of 47%.^[14] For cyclohexanol, they observed glutaric and succinic acids as by-products, which could also be confirmed by our group for methyl-substituted cyclohexanols.^[15] Herein, we present significant improvements in scaling up such electrooxidations, tackling miscibility challenges for biphasic reaction mixtures and enhancing the product yield via substrate feeding. Lastly, we revised the reported reaction mechanism and propose changes how the radical mechanism at a nickel oxyhydroxide anode likely leads to oligomeric species, not described earlier.

Results and Discussion

We investigated the electrochemical conversion of the alicyclic alcohol **1** into the corresponding adipic acid **2** (Scheme 1).

An efficient approach to quickly identify significant parameters which affect the product yield is a *Design of Experiments* (DoE) parameter screening.^[16] Since an active nickel foam anode and a stainless steel cathode are superior electrode materials for this reaction, as previously shown by Rauen et al.,^[15] optimization focused on the activation parameters of the nickel foam (current density and applied charge), the current density and applied charge during the reaction, as well as substrate concentration, mixing with the electrolyte, and reaction temper-



Scheme 1. Anodic oxidation of 4-propylcyclohexanol (**1**) to 3-propyladipic acid (**2**) at nickel oxyhydroxide foam anodes.

Table 1. Parameters of 2^{7-3} DoE screening with a resolution of IV. Seven parameters and their interactions were checked: substrate concentration ($C_{\text{substrate}}$), reaction temperature (T), mixing speed with a magnetic stirring bar (v_{mix}), reaction current density (j_{rct}), total applied charge for the reaction (Q_{rct}), current density for activation (j_{act}) and applied charge for the activation (Q_{act}). With two replications and two center point experiments, 34 experiments were performed. Other parameters: 1 M NaOH_(aq) as the electrolyte, total reaction volume: $V_{\text{tot}} = 100$ mL, anode geometric surface area $A_{\text{anode}} = 72$ cm².

$C_{\text{substrate}}/$ m ^[a]	$T/$ °C ^[b]	$v_{\text{mix}}/$ rpm ^[c]	$j_{\text{rct}}/$ mA cm ^{-2[d]}	$Q_{\text{rct}}/$ F	$j_{\text{act}}/$ mA cm ^{-2[d]}	$Q_{\text{act}}/$ C cm ^{-2[d]}
0.3	40	200	6	6.5	3.5	0.5
0.4	50	350	7	7.0	5.0	5.5
0.5	60	500	8	7.5	6.5	10.5

[a] Initial concentration of 4-propylcyclohexanol. [b] Temperature set in the thermostat. [c] A cylindrical magnetic stirring bar was used. [d] The values refer to the anode geometric surface area.

ature. All parameters, corresponding to both anode activation and reaction, their corner values, and central points are listed in Table 1 (first row):

All experiments were analyzed using ¹³C Inverse Gated NMR spectroscopy, with 1,3,5-trimethoxybenzene as an internal standard. The individual results are presented in the supporting information (supporting information, Table S1). Hereafter, a summary of the DoE results is shown in a main effects plot, where all the trends for the tested parameters are presented (Figure 1). Thereby, parameter trends that lie below the significance level are highlighted in grey. Thus, their effect on the product yield in the tested range is insignificant for the tested setup.

The favorable trends towards higher temperatures (60 °C) and higher stirring speeds (500 rpm) both lead to higher phase exchange rates. The Pareto chart (Figure 2) displays the relative significance of all parameters.

These results in particular point out the importance of mixing: at an increased temperature of 60 °C and under vigorous stirring as the yield significantly increases. A previous report revealed that elevated temperatures were unfavorable to

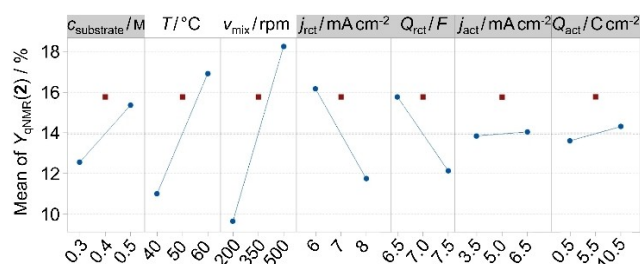


Figure 1. Main effects plot of the Design of Experiments (DoE) screening applying a 2^{7-3} -design with a resolution of IV. The R^2 value for an α -value of 0.05 is 28%. Corner points are represented by blue circles, and center points by red squares. A grey background represents a term not included in the model.

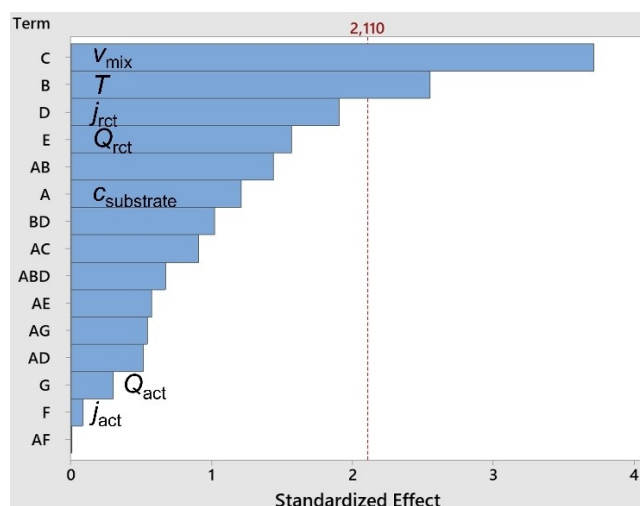


Figure 2. Pareto chart of the first DoE screening results. The most significant effects on the product yield are triggered by the stirring speed (term C) and the reaction temperature (term B). The current density (D), applied charge (E), other parameters, and parameter interactions are below the significance level of $\alpha = 0.05$. The R^2 value is 28%.

achieve higher yields, which is one reason why the temperature was not enhanced further.^[15] The screening of higher current densities than those reported previously^[15] showed a downward yield trend for this substrate. Likewise, the applied charge value showed a downward trend. The data indicates this trend in a value range beneath the theoretically required 8.0 *F*. Therefore, the summarily presented trend may be a sum of fluctuations or it may indicate that side reactions take place which require less charge than the productive pathway. Since this parameter is of lower significance, we focused on the most influential ones instead, namely temperature and stirring speed. This observation has led to the implementation of an eductor, which allows efficient mixing of the alcohol 1 and the aqueous electrolyte, as its solubility is quite low (675.8 mg alcohol/L water, at 20 °C, Figure 3).

We tested the mixing of two immiscible phases with a commercially available eductor piece (Figure 4), which is a mixing device using the Venturi effect.^[17]

This biphasic electrolyte system uses the bottom flow of the aqueous layer (1 M NaOH_(aq)) to suck the above-lying organic phase (4-propylcyclohexanol) in a designed junction. The diameters of the two inflows are intentionally different to induce a pressure drop and a liquid suction (Venturi effect). The resulting turbulence becomes more significant with increasing flow rates. A model system consisting of iodine-colored cyclohexane and water was employed to verify the mixing properties of this setup. The resultant mixture appeared to be

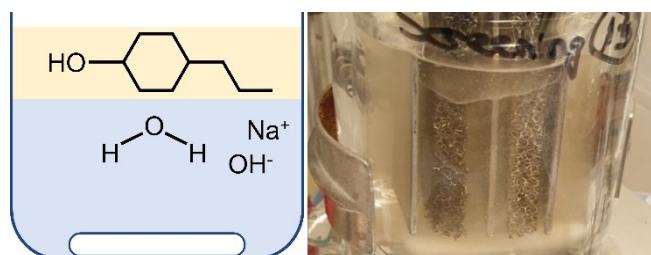


Figure 3. Left: Sketch of the naturally biphasic system of the electrolyte components 1 and caustic soda. Right: Photo taken during an electrolysis during which the biphasic system is visible.

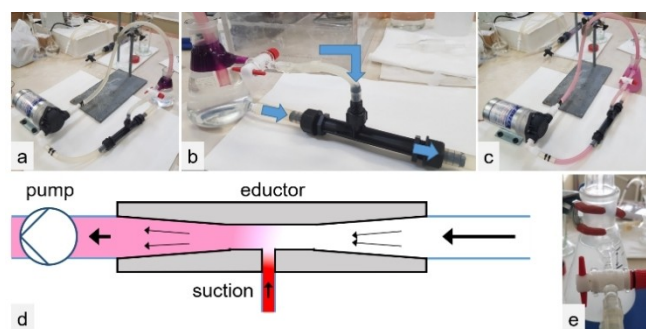


Figure 4. a–c: An emulsification test with an eductor was performed. To facilitate the visualization of emulsification, an iodine-colored organic phase (cyclohexane) and water were used. Whether phases were separating afterward, or a temporarily stable phase mixture was achieved, could thereby be tested. d: Sketch of the working principle of an eductor piece, using the Venturi effect. e: Final emulsified reaction mixture.

homogeneous, confirming the emulsification function. The real electrolyte system also resulted in a homogenous dispersion of the alcohol in the aqueous solution. We could show that flow rates of 250 and 65 Lh⁻¹ are both sufficient for the generation of an emulsion of the substrate and the aqueous solution for 12 h. Prior to conducting another *DoE* screening with improved mixing properties, the setup was modified to work in a semi-batch mode. Thereby, constant emulsification was ensured, even for experiments that lasted longer than 12 h. With this in hand, the setup was modified to a semi-batch one. Towards this goal, the commercially available 100 mL batch-type cell was modified to include two channels: one enabling the inlet to the reaction volume, and the other for the outflow (Figure 5). From the reservoir (a 100 mL measuring cylinder), two tubes fed the mixing eductor, from where a membrane pump forwarded the mixture to the reactor. The outflow was connected to the reservoir.

The tested parameters with the modified setup were substrate concentration and flow rate (Table 2). Hereby, the flow rate was further decreased so that the flow drives both the emulsification and the transport of the reaction mixture (Figure 6).



Figure 5. The transition from the batch-type cell for the first *DoE* (left) to the semi-flow mode electrolysis cell for the second *DoE* screening (right).

Table 2. Parameters of 2² *DoE* screening with full resolution. One center point and one repetition per experiment were implemented. A set of 10 experiments was performed. Other parameters: 1 M NaOH_(aq) as the electrolyte, total reaction volume: $V_{\text{tot}} = 250$ mL, applied current density $j_{\text{reaction}} = 5$ mAcm⁻², applied charge $Q_{\text{reaction}} = 8.5$ *F*, stirring speed with magnetic stirring bar: $v_{\text{mix}} = 500$ rpm, anode geometric surface area $A_{\text{anode}} = 128$ cm², reaction temperature $T_{\text{reaction}} = 60$ °C, nickel foam activation with $j_{\text{act.}} = 7.5$ mAcm⁻² and $Q_{\text{act.}} = 5$ Ccm⁻².

$c_{\text{substrate}}/\text{m}^{\text{[a]}}$	$\phi/\text{L h}^{-1\text{[b]}}$
0.4	2*
0.55	16
0.7	30

[a] Initial concentration of 4-propylcyclohexanol. [b] The flow rate was set with a Ritmo R033 membrane pump by Fink Chem + Tec, located between the mixing eductor and the reactor. *For one experiment, a flow of 5 Lh⁻¹ was set, since with the initially set flow rate, the electrolyte repeatedly stopped flowing after a few minutes of pumping.

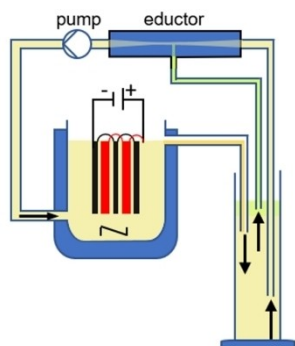


Figure 6. Schematic of the semi-batch setup for the second *DoE* screening. The pump transports the reaction medium and ensures a flow rate for successful emulsification inside the eductor. The eductor has two inlet channels, to continuously mix the two liquid electrolyte phases in the reservoir (100 mL). The product formation takes place in the electrochemical continuous stirred tank reactor (e-CSTR).

The parameter concentration was tested once more, now with an emphasis on higher values. This decision was based on the slightly positive trend towards higher substrate concentrations in the first *DoE* and motivated by a possibly reduced amount of caustic soda per unit of produced **2**.

For these experiments, the ^{13}C Inverse Gated NMR quantification was performed after liquid-liquid extraction using a perforator, as done previously. The detailed results are listed in the supporting information (supporting information, Table S2). These *DoE* screening results display that the stability of the emulsion is still crucial, with high pumping speeds affecting the yield. The optimal result during this screening was a qNMR yield of 35% for **2**. This screening prompted a kinetic investigation of the transpiring reaction (**1** to **2**). The upscaling of the system was also addressed.

For the kinetic study, a larger reaction volume is advantageous, because i) the volume of the withdrawn samples does not significantly affect the total volume and concentration, and ii) kinetic effects may arise as a result of scaling up. For these reasons, the electrode stack was enlarged by a factor of nearly 10 in terms of total geometrical anode surface area ($A_{\text{geom.}} = 1225 \text{ cm}^2$, equal geometrically active cathodic surface area), in part by increasing the number of individual electrodes (Figure 7). Thus, five anode foams and six stainless-steel sheet electrodes were assembled and respectively connected for one electrode stack. This setup has the additional advantage that both sides of the anodes are electrochemically active. A commercially available 1.5 L glass vessel with a heating jacket by *HWS* was used as a reactor and a custom-made PTFE cap was employed for the installation of the electrode stack. A commercially available 10 L glass reactor with an agitator unit and a heating jacket by *Normag*TM was installed as a reservoir.

With this setup, experiments with a total reaction volume of up to 13 L were conducted and samples were taken to observe the product composition or other kinetic effects during the reaction (Figure 8).

Figure 9 shows an overview of the results obtained from the product composition analysis in the course of the electro-



Figure 7. Bottom view of the electrode stack. The nickel foam sides are separated from the stainless-steel cathodes by screws made of polyether ether ketone (PEEK, thickness per side 3 mm). The anode geometric surface area in contact with the electrolyte is 1225 cm^2 . The foams have a thickness of 5 mm. The stainless-steel sheets have a thickness of 1 mm.



Figure 8. Reaction setup of the upscaled e-CSTR. Left: tempered reservoir with agitator. Below: thermostat. Above: eductor piece in black. Right: reactor with electrode stack. Behind: membrane pump. In the background, an Erlenmeyer flask with fresh substrate and a peristaltic pump for substrate feeding are installed. The overall reaction volume is up to 13 L. The yellow color of the reaction mixture in a later reaction stage can be visually perceived.

chemical reaction, with the samples taken at different values of applied charge.

The oxidation from **1** to **2** was previously proposed to take place via the formation of 1,3- and 1,4-cyclohexanediones as intermediates to glutaric and succinic acids.^[18] However, with our alkylated substrates, this would result in 4-propyl-4-hydroxy-cyclohexane-1-one, which is not observed. Also, the tautomeric appearance of the corresponding enol form was not detected. In addition, propylsuccinic acid cannot form via this

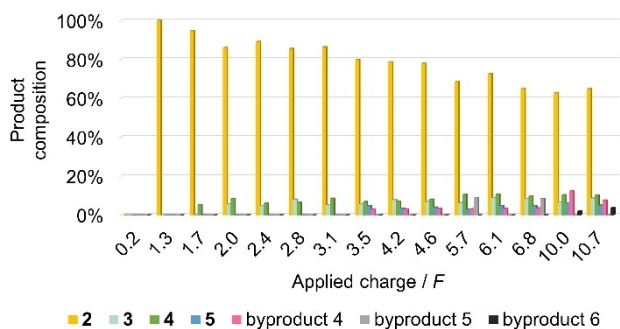


Figure 9. Analysis of the product composition throughout the reaction. Applied parameters: 1 M NaOH_(aq) as the electrolyte, substrate concentration $c(1) = 0.2$ M, total reaction volume $V_{\text{tot}} = 3.1$ L, reaction mixture flow rate $\Phi_{\text{reaction}} = 16$ L h⁻¹, applied current density $j_{\text{reaction}} = 2.5$ mA cm⁻², applied charge $Q_{\text{reaction}} = 10.7$ F, stirring speed with magnetic stirring bar $v_{\text{mix}} = 300$ rpm, anode geometric surface area $A_{\text{anode}} = 1225$ cm², reaction temperature $T_{\text{reaction}} = 50$ °C, nickel foam activation with $j_{\text{act.}} = 6.5$ mA cm⁻² and $Q_{\text{act.}} = 5$ C cm⁻². The main product (2) as well as further reported alkylated dicarboxylic acid derivatives^[15] form in the case of the propyl side chain during the reaction. In a later reaction stage, further dicarboxylic acids arise, which can be observed in the ¹³C NMR spectrum but not conclusively characterized.

intermediate. We observed propylsuccinic acid in an NMR yield of up to 6% (Figure 9). Accordingly, a revision to the previous mechanism is unavoidable. We propose a reaction mechanism by subsequent oxidation steps in 1,2-positions. A yellow-colored product solution would fit the supplier information of cyclohexanedione^[19] or the bright yellow color of 2. However, the concentrated product mixture after extraction and solvent removal turned out to be dark orange. Also, an even darker distillation residue remains as a sticky solid. While ¹³C NMR analyses revealed that the main product 2 seems to be the only compound left, a MALDI ToF MS measurement (supporting information, Figure S7) indicates the formation of high molecular weight compounds. Their end groups should be acidic, according to pH measurements and the fact that they dissolve reversibly in caustic soda. The mechanism we propose here focuses on the interaction with the strongly alkaline electrolyte (Scheme 2). This influence may also be a reason for higher molecular weight by-products being formed.

Importantly, the NMR studies (Figure 9) reveal that, initially, the main product 2 is exclusively formed. Only after 1.7 F was 4 characterized as the first formed by-product. Within another 0.3 F, 3 was observed in the NMR spectrum. The next by-product was 5, which was detected after 3.5 F, and over the course of the reaction, more by-products were seen in the ¹³C Inverse Gated NMR spectrum and identified as dicarboxylic acids. Quantification was done by integrating the signals in the chemical shift range of the carboxylic acids, whereby equal integrals for two acid signals were observed in several spectra. Overlapping signals and low quantities of the other by-products have prohibited their identification so far.

A quantitative study was performed next, with samples taken every 3 h, worked up as described in the experimental section. The overview is presented in Figure 10.

As known from the literature^[20], 1' forms as an intermediate at the beginning of the reaction. When most of the starting

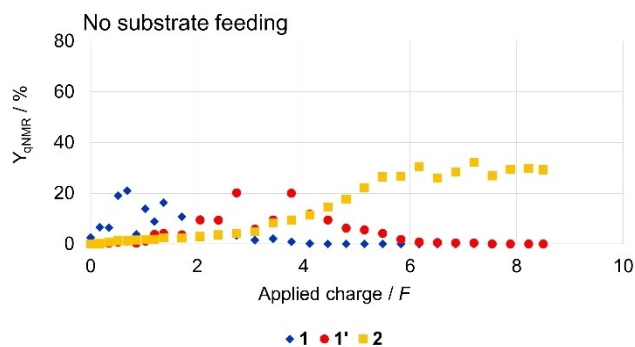


Figure 10. qNMR yields of the reaction control experiment for the oxidation from 1 to 2 via 1'. The volatilities of 1 and 1' are the reason for lowered ascertained yields, especially in the early reaction stage. Samples were taken every 3 h and the qNMR yields were evaluated. Reaction parameters: The total reaction volume was $V_{\text{tot}} = 3.9$ L. The amount of substrate was $n(1) = 2.0$ mol, and the nominal reagent concentration was $c(1) = 0.55$ M in 1 M NaOH_(aq). A reaction temperature of $T = 60$ °C and a current density of $j_{\text{act.}} = 5$ mA cm⁻² were applied. The reaction mixture was pumped from the reservoir through a mixing eductor into the reactor with a flow rate of 16 L h⁻¹. For recirculation, the reaction mixture was flowing back into the reservoir.

material is depleted, there is a maximum in the intermediate yield (Figure 10). The production of 2 from 1' causes a maximum space-time yield of 2 at a later reaction stage, namely where the curvature is zero. Thus, the idea arose to start from 1' (Scheme 3) for simplicity and availability reasons and to feed 1' to the system continuously with a flow rate equal to the theoretically maximum oxidation rate. This corresponds to 0.59 mmol min⁻¹, or 9.8 μL min⁻¹.

The evaluation of this reaction control experiment is shown in Figure 11.

Remarkably, the main product 2 shows a nearly proportional increase in yield, when the substrate concentration is

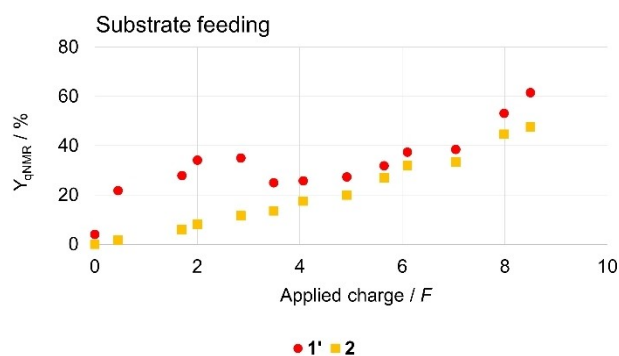
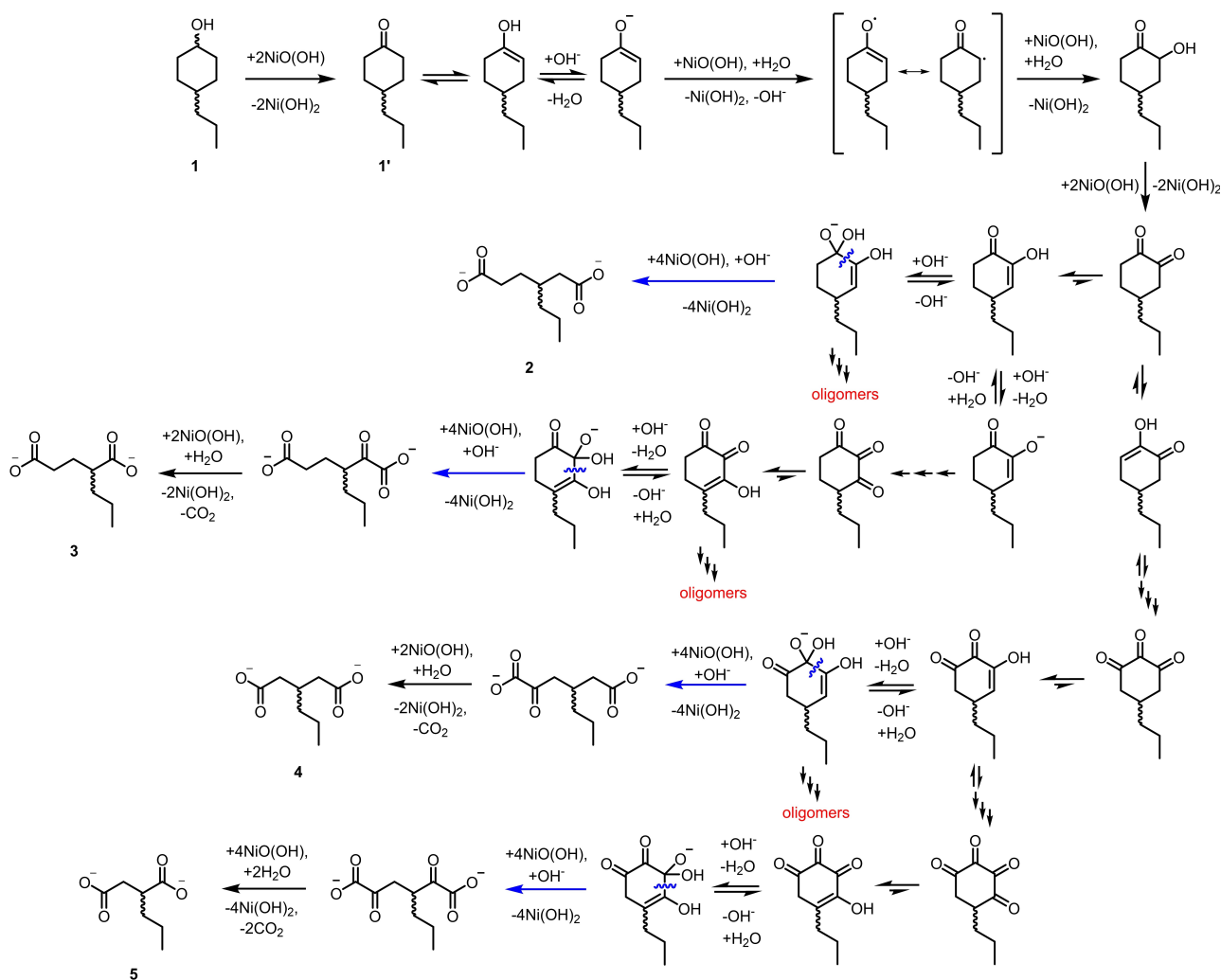
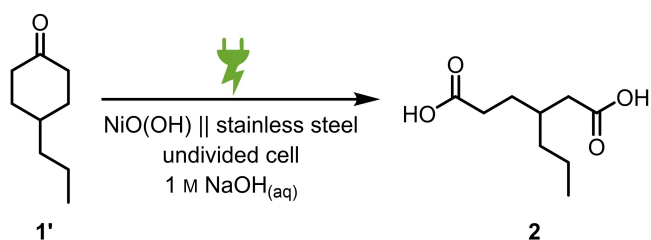


Figure 11. qNMR yields for the reaction control experiment consisting of the anodic oxidation from 1' to 2 with continuous substrate feeding for a constant concentration. The volatility of 1' is the reason for a lowered ascertained yield, especially in the early reaction stage. Overall, constant feeding of 1' should correlate to a stable value of the red data points. Instead, the values fluctuate, because of the compound's volatility during mini workup. Samples were taken regularly and the qNMR yields were evaluated. Reaction parameters: The total reaction volume was $V_{\text{tot}} = 10.0$ L and the initial amount of substrate was $n(1') = 5.1$ mol. The yields were evaluated against this stoichiometry. Beyond 8 F, the respective initial amount of substrate was linearly increased according to the theoretical maximal conversion.



Scheme 2. Reaction mechanism from 4-propylcyclohexanol (1) via 4-propylcyclohexanone (1') to 3-propyladipic acid (2). Fleischmann et al. reported the oxidation from 1 to 1'.^[20] Its radical nature and mechanism was further investigated by Konaka et al.^[21] The keto-enol tautomerization with subsequent deprotonation was reported by Schäfer et al.^[13] At the nickel oxyhydroxide surface, the oxidation to the corresponding radical was proposed by Lyalin et al.^[14] The next two oxidation steps as well as the water addition were reported by the same group.^[22] The tautomerization of 1' and 4-propylcyclohexane-1,2-dione to their enol forms proceed for the same reason. From an enol form, there is a higher tendency for another oxidation in the 3-position. In contrast, starting from the enol form a nucleophilic attack of hydroxide can also initiate a ring opening. Furthermore, we propose a reaction pathway toward oligomers, since the double bond is electrophilic. The dicarboxylic acids are in their dianion form.



Scheme 3. Anodic oxidation of 4-propylcyclohexanone (1') to 3-propyladipic acid (2) at a nickel oxyhydroxide foam anode.

kept constant. Additionally, the product yield was shown to significantly increase from about 30% to almost 50% qNMR yield. Thus, substrate feeding can be considered a particularly relevant parameter for increasing the yield of the oxidation of 1' to 2. After workup and isolation of 2, 31% remained. The ¹H

and ¹³C NMR spectra of the black, sticky distillation residue exclusively showed signals that are ascribable to 2. Still, the remaining 2 could not be successfully removed from the distillation residue. The exact chemical composition of the distillation residue and its behavior is a topic of an ongoing investigation.

Conclusions

In summary, we showed the successful isolation of 3-propyladipic acid from 4-propylcyclohexanol and 4-propylcyclohexanone with isolated yields of up to 31% on a 10 L scale, corresponding to 48% qNMR yield. In an initial parameter screening, the importance of the biphasic electrolyte mixing emerged. Utilizing a mixing eductor, an emulsion resulted.

Upon switching to a recirculation reaction mode, more detailed information was obtained from another *Design of Experiments* screening, pointing to the critical importance of electrolyte emulsification. When the scale-up to a reaction volume of up to 10 L was conducted, reaction control experiments revealed significant yield improvements when continuously feeding the substrate. Optically, the reaction progress was accompanied by the coloring of the electrolyte, which resulted in yellow to red mixtures upon reaction completion. Thereby, the shade deepening correlated with the reaction time. Analyses indicated that the color results from trace compounds of high molecular weight. For their formation, the following mechanistic proposal was presented: The keto-enol tautomerization is favored in cyclohexane-1,2-diones. Due to the mesomeric effect of the carbonyl group, the unsaturated α -carbon is more electrophilic in comparison with a saturated one. Consequently, other nucleophiles can attack this position, initiating a chain reaction. This hypothesis is an interesting starting point for further studies at the nickel oxyhydroxide anode surface. There is significant room for the optimization of the electrocatalyst surface by tailoring the surface structure and composition. This combined with an in-depth knowledge of the prevailing mechanisms should allow for rational progress in organic electrosynthesis.

In a more general vein, these results can contribute to transforming the production of **2** to be more climate friendly. Hence, in the future, it will be relevant to check the effects of renewable energy source fluctuations on the yield. In favorable cases, it may be practical to use electricity from renewable energies immediately upon their conversion.

Experimental Section

General considerations

Experimental details, information about the analyses, and further information is presented in the Supporting information.

Activation of nickel foams

As reported by Briggs et al.^[23] and Schäfer et al.^[13], an activation solution which is 0.1 M NiSO_{4(aq)}, 0.1 M NaOAc_(aq) and 5 mM NaOH_(aq) was placed in a beaker-type cell, previously cleaned. A simpler reaction setup was used to do the activation in batch mode. The reactor stack was assembled, and the nickel foam anodes were thoroughly rinsed with 1 M caustic soda. Once the caustic soda was not dripping any more, the electrode stack was inserted into the activation solution. Thereby some floccules were observed, which do not hinder the activation. The activation was performed galvanostatically with a current density of 7.5 mA cm⁻² until attaining an applied charge of 5 C cm⁻², unless stated differently. The activation mixture was stirred at 300 rpm. Then, the electrode stack was disassembled, and the black activated nickel foams were rinsed thoroughly with deionized water. The stainless-steel plates were immersed in diluted H₂SO_{4(aq)} (1–4 M) for a few seconds, washed with water, dried with a tissue, and treated with sandpaper (pore sizes: first 700, then 300). The shiny stainless-steel plates were rinsed with water, acetone and water once more, dried and the cell rearranged.

Setup

For the applied electrode stack, three (or six) stainless steel (alloy type EU norm 1.4571) plates were connected by thin stainless-steel plates, and two (or five) RECEMAT™ nickel foams RCM-Ni4753.05 were also connected by such stainless-steel plates. Since the geometrical surface area of both sides of the anodes was used, one additional cathode was needed. All electrodes were separated by 3 mm thin PTFE spacers, strung on two PTFE cylinders for stability reasons. The stainless-steel sheets were equipped with 3 mm thick polyether ether ketone (PEEK) screws to ensure a homogeneous spacing throughout the large electrode stack.

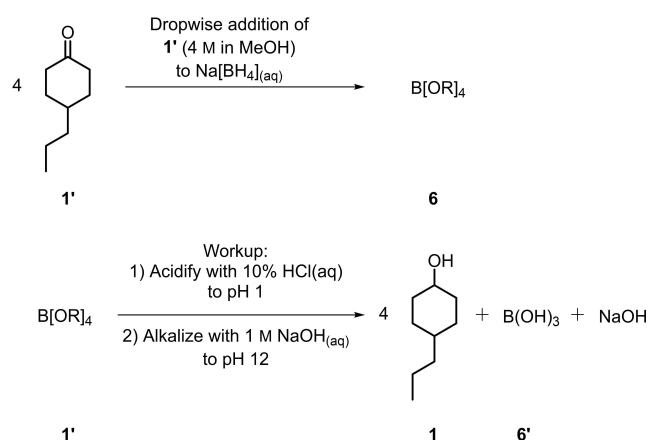
For the first *DoE* screening, a small electrode stack was combined with a commercially available 100 mL batch-type electrolysis cell. For the second screening, in- and outflow channels were added to the beaker-type electrolysis cell. For the large-scale electrolysis, a commercially available 1.5 L beaker-type electrolysis cell by HWS was used. Here, the inflow channel was already a preset and a PTFE lid with an outlet channel and an opening for the electrode stack was tailor-made by the machine workshop at the university of Mainz.

Synthesis of 4-propylcyclohexanol

For availability reasons, 4-propylcyclohexanone (**1'**, 1.651 mol) was reduced to the main substrate 4-propylcyclohexanol (**1**) using sodium borohydride (0.826 mol, 2 H⁻ equivalents) in deionized water (250 mL, Scheme 4). **1'** in methanol (123 mL) was added dropwise (1 drop in 4 sec) to the aqueous solution. The reaction mixture was stirred at 300 rpm. After the completed addition, the reaction was continuously stirred for another 20 h. The reaction progress was observed using TLC (eluent was toluene, coloring agent: vanillin/sulfuric acid, R_f(**1'**)=0.64, R_f(**6**)=0.28). Upon the completed conversion, the turbid reaction mixture was acidified using either hydrochloric acid (10%) or sulfuric acid (4.5 M) to pH 1–2. Subsequently, a 1 M NaOH solution was added until reaching a pH of 12. After threefold extraction using methyl *tert*-butyl ether (MTBE), the combined organic phases were dried over MgSO₄ and the solvent was removed at reduced pressure. **1** was synthesized with a yield of 96%.

Anodic oxidation of 4-propylcyclohexanol

4-Propylcyclohexanol (**1**, isomeric mixture) was mixed with caustic soda (1 M). The activated electrode stack was inserted into the



Scheme 4. Reduction of **1'** with sodium borohydride, including the subsequent workup.

stirred reaction mixture. In the case of a semi-flow reaction, the recirculation of the reaction mixture was established before starting the reaction. After the galvanostatic reaction ended, the product mixture was collected, and the setup and electrode stack were washed and thoroughly rinsed with MTBE (several mL, enough for pumping) and NaOH (1 M), respectively. All phases were combined and worked up.

Reaction control experiments and mini workup

4-Propylcyclohexanone ($\geq 99\%$) was chosen as the substrate as it could be characterized as the first intermediate in the reaction pathway via NMR spectroscopy and it was readily available. Regarding the further reaction steps, the same parameters were applied as before, unless stated differently. During the reaction, (2.00 \pm 0.05) mL of the reaction mixture was retrieved regularly with a syringe, acidified with 4.5 M H₂SO_{4(aq)} to pH 1–2, and extracted with ethyl acetate (4 times, 2 mL each). The organic fractions were combined and dried over MgSO₄. Then, the solvent was evaporated at reduced pressure, the residue combined with 1,3,5-trimethoxybenzene as an internal standard, DMSO-d₆ (0.5 mL) was added, and the solution was analyzed using ¹³C Inverse Gated NMR spectroscopy.

General workup

The combined phases in the product mixture were inserted in a sufficiently large perforator according to Ludwig (at least 20% extra spare volume) and a liquid-liquid reaction was performed, first using MTBE until completely discolored. After acidification with diluted H₂SO_{4(aq)} (4.5 M) to pH 1–2, the dicarboxylic acid product mixture was liquid-liquid extracted with the same perforator using ethyl acetate until completely discolored. The two organic fractions were dried over MgSO₄, the solvent was removed at reduced pressure and the product mixture was evaluated using ¹³C Inverse Gated NMR spectroscopy with 1,3,5-trimethoxybenzene as an internal standard.

For isolation, the acidic mixture was distilled using a Vigreux column at 10⁰–10^{–2} mbar. The products were trapped with liquid nitrogen by using a Schlenk flask. The main product **2** was distilled at about 200 °C. The purity was significantly improved by recrystallization in heptane after first melting the yellow crystals in a heptane phase on a hot plate at about 70 °C, and slowly cooling to room temperature. Then, the crystals were dried.

Supporting Information

An additional reference was cited within the Supporting Information.^[24]

Acknowledgements

We thank the analytical departments of Johannes Gutenberg University Mainz and the University of Alicante for the measurements and fruitful discussions. Additionally, we are grateful for the support of the glass workshop of the university of Mainz.



This project has received funding from the European Union's Horizon 2020 research and innovation programme

under grant agreement no. 820735. This publication reflects the views only of the author, and the European Union cannot be held responsible for any use which may be made of the information contained therein.

The authors declare no competing financial interest. Open Access funding enabled and organized by Projekt DEAL.

Conflict of Interests

The authors declare no conflict of interest.

Data Availability Statement

The data that support the findings of this study are available in the supplementary material of this article.

Keywords: carboxylic acids · electrocatalysis · electrochemistry · oxidation · renewable resources

- [1] F. Birol, L. Cozzi, M. Baroni, T. Morgan, A. Bromhead, M. Argiri, J. Corben, P. Olejarnik, C. Besson, A. Blasi, R. Centurelli, M.-X. Chen, M. D'Ausilio, D. Elis, M. Frank, T. Gould, T. Gül, K. Kumaria, Q. Liu, B. Magné, T. Malyshev, T. Topalgoekceli, D. Wilkinson, A. Yanagisawa, S. Mooney, International Energy Agency, and Fatih Birol. World energy outlook 2010, Paris.
- [2] S. A. Matlin, G. Mehta, H. Hopf, A. Krief, *Nat. Chem.* **2016**, *8*, 393–398.
- [3] a) S. R. Waldvogel, B. Janza, *Angew. Chem. Int. Ed.* **2014**, *53*, 7122–7123; b) B. Gleede, M. Selt, C. Gütz, A. Stenglein, S. R. Waldvogel, *Org. Process Res. Dev.* **2020**, *24*, 1916–1926; c) D. Hayrapetyan, V. Shkepu, O. T. Seilkhanov, Z. Zhanabil, K. Lam, *Chem. Commun.* **2017**, *53*, 8451–8454; d) T. Noël, Y. Cao, G. Laudadio, *Acc. Chem. Res.* **2019**, *52*, 2858–2869; e) M. Yan, Y. Kawamata, P. S. Baran, *Chem. Rev.* **2017**, *117*, 13230–13319; f) M. C. Leech, K. Lam, *Nat. Chem. Rev.* **2022**, *6*, 275–286; g) M. Zirbes, T. Graßl, R. Neuber, S. R. Waldvogel, *Angew. Chem. Int. Ed.* **2023**, *62*, e202219217; h) A. Wiebe, T. Gieshoff, S. Möhle, E. Rodrigo, M. Zirbes, S. R. Waldvogel, *Angew. Chem. Int. Ed.* **2018**, *57*, 5594–5619; *Angew. Chem. Dev.* **2018**, *130*, 5694–5721; i) S. Möhle, M. Zirbes, E. Rodrigo, T. Gieshoff, A. Wiebe, S. R. Waldvogel, *Angew. Chem. Int. Ed.* **2018**, *57*, 6018–6041; j) S. Möhle, M. Zirbes, E. Rodrigo, T. Gieshoff, A. Wiebe, S. R. Waldvogel, *Angew. Chem.* **2018**, *130*, 6124–6149; k) K. D. Moeller, *Chem. Rev.* **2018**, *118*, 4817–4833; l) R. D. Little, K. D. Moeller, *Chem. Rev.* **2018**, *118*, 4483–4484; m) S. R. Waldvogel, S. Lips, M. Selt, B. Riehl, C. J. Kampf, *Chem. Rev.* **2018**, *118*, 6706–6765.
- [4] D. Pollok, S. R. Waldvogel, *Chem. Sci.* **2020**, *11*, 12386–12400.
- [5] a) S. B. Beil, D. Pollok, S. R. Waldvogel, *Angew. Chem. Int. Ed.* **2021**, *60*, 14750–14759; b) J. Seidler, J. Strugatchi, T. Gärtner, S. R. Waldvogel, *MRS Energy Sustainability* **2020**, *7*, 42.
- [6] a) E. J. Horn, B. R. Rosen, Y. Chen, J. Tang, K. Chen, M. D. Eastgate, P. S. Baran, *Nature* **2016**, *533*, 77–81; b) E. J. Horn, B. R. Rosen, P. S. Baran, *ACS Cent. Sci.* **2016**, *2*, 302–308; c) L. J. Wesenberg, E. Diehl, T. J. B. Zähringer, C. Dörr, D. Schollmeyer, A. Shimizu, J.-i. Yoshida, U. A. Hellmich, S. R. Waldvogel, *Chem. Eur. J.* **2020**, *26*, 17284–17612; d) M. Linden, S. Hofmann, A. Herman, N. Ehler, R. M. Bär, S. R. Waldvogel, *Angew. Chem. Int. Ed.* **2023**, *62*, e202214820; e) J. Winter, T. Prenzel, T. Wirtanen, D. Schollmeyer, S. R. Waldvogel, *Chem. Eur. J.* **2023**, *29*, e202203319; f) R. J.-R. Bednarz, C. Brauer, S. R. Waldvogel, *GIT Lab. J.* **2021**, online.
- [7] a) J. L. Röckl, D. Schollmeyer, R. Franke, S. R. Waldvogel, *Angew. Chem. Int. Ed.* **2020**, *59*, 315–319; *Angew. Chem.* **2020**, *132*, 323–327; b) S. Arndt, D. Weis, K. Donsbach, S. R. Waldvogel, *Angew. Chem. Int. Ed.* **2020**, *59*, 8036–8041; *Angew. Chem.* **2020**, *132*, 8112–8118.
- [8] a) K.-F. Chow, F. Mavré, J. A. Crooks, B.-Y. Chang, R. M. Crooks, *J. Am. Chem. Soc.* **2009**, *131*, 8364–8365; b) S. E. Fosdick, K. N. Knust, K. Scida, R. M. Crooks, *Angew. Chem. Int. Ed.* **2013**, *52*, 10438–10456; c) G. H. M. de Kruijff, T. Goschler, N. Beiser, A. Stenglein, O. M. Türk, S. R. Waldvogel, *Green Chem.* **2019**, *21*, 4815–4823.

- [9] L. Gustavsson, B. Johansson, P. Svenningsson, *Energy* **1995**, *20*, 1097–1113.
- [10] A. Corona, M. J. Bidy, D. R. Vardon, M. Birkved, M. Hauschild, G. T. Beckham, *Green Chem.* **2016**, *18*, 1839–1854.
- [11] W. Schutyser, G. Van den Bossche, A. Raaffels, S. Van den Bosch, S.-F. Koelewijn, T. Renders, B. F. Sels, *ACS Sustainable Chem. Eng.* **2016**, *4*, 5336–5346.
- [12] a) M. Zirbes, S. R. Waldvogel, *Curr. Opin. Green Sustain. Chem.* **2018**, *14*, 19–25; b) M. Zirbes, L. L. Quadri, M. Breiner, A. Stenglein, A. Bomm, W. Schade, S. R. Waldvogel, *ACS Sustainable Chem. Eng.* **2020**, *8*, 7300–7307; c) M. Breiner, M. Zirbes, S. R. Waldvogel, *Green Chem.* **2021**, *23*, 6449–6455; d) M. Zirbes, D. Schmitt, N. Beiser, D. Pitton, T. Hoffmann, S. R. Waldvogel, *ChemElectroChem* **2019**, *6*, 155–161.
- [13] H.-J. Schäfer, J. Kaulen, *Tetrahedron* **1982**, *38*, 3299–3308.
- [14] B. V. Lyalin, V. A. Petrosyan, *Russ. Chem. Bull.* **2004**, *53*, 688–692.
- [15] A. L. Rauen, F. Weinelt, S. R. Waldvogel, *Green Chem.* **2020**, *22*, 5956–5960.
- [16] a) M. Hielscher, E. K. Oehl, B. Gleede, J. Buchholz, S. R. Waldvogel, *ChemElectroChem* **2021**, *8*, 3904–3910; b) M. Dörr, M. M. Hielscher, J. Proppe, S. R. Waldvogel, *ChemElectroChem* **2021**, *8*, 2621–2629; c) M. Dörr, J. L. Röckl, J. Rein, D. Schollmeyer, S. R. Waldvogel, *Chem. Eur. J.* **2020**, *26*, 10195–10198; d) M. Santi, J. Seitz, R. Cicala, T. Hardwick, N. Ahmed, T. Wirth, *Chem. Eur. J.* **2019**, *25*, 16230–16235; e) R. Möckel, J. Hille, E. Winterling, S. Weidemüller, T. M. Faber, G. Hilt, *Angew. Chem. Int. Ed.* **2018**, *57*, 442–445; *Angew. Chem.* **2018**, *130*, 450–454.
- [17] a) H. Li, H. Li, X. Huang, Q. Han, Y. Yuan, B. Qi, *Processes* **2020**, *8*, 64; b) M. Georgiou, M. V. Papalexandris, *Int. J. Heat Mass Transf.* **2017**, *115*, 793–809.
- [18] B. V. Lyalin, V. A. Petrosyan, *Russ. Chem. Bull.* **2009**, *58*, 2426–2431.
- [19] a) C. C. Hach, C. V. Banks, H. Diehl, *Org. Synth.* **1952**, *32*, 35; b) Sigma-Aldrich, Safety Data Sheet for 1,2-cyclohexanedione, 2022, CAS-No. 765-87-7, <https://www.sigmaaldrich.com/DE/en/sds/aldrich/w345806>, last accessed: 08.08.2023.
- [20] M. Fleischmann, K. Korinek, D. Pletcher, *J. Electroanal. Chem. Interfacial Electrochem.* **1971**, *31*, 39–49.
- [21] R. Konaka, S. Terabe, K. Kuruma, *J. Org. Chem.* **1969**, *34*, 1334–1337.
- [22] B. V. Lyalin, V. A. Petrosyan, *Russ. J. Electrochem.* **2010**, *46*, 1199–1214.
- [23] G. W. D. Briggs, E. Jones, W. F. K. Wynne-Jones, *Trans. Faraday Soc.* **1955**, *51*, 1433–1442.
- [24] W. L. F. Armarego, *Purification of Laboratory Chemicals: Part 2 Inorganic Chemicals, Catalysts, Biochemicals, Physiologically Active Chemicals, Nanomaterials*, Butterworth-Heinemann, **2022**..

Manuscript received: May 2, 2023

Revised manuscript received: June 30, 2023

Accepted manuscript online: July 16, 2023

Version of record online: August 10, 2023